Joint characterization of the vegetation by satellite observations from visible to microwave wavelengths: A sensitivity analysis

Catherine Prigent
Department of Applied Physics, Columbia University, NASA Goddard Institute for Space Studies, New York, New York

Filipe Aires
Department of Applied Physics, Columbia University, NASA Goddard Institute for Space Studies, New York, New York

William Rossow
NASA Goddard Institute for Space Studies, New York, New York

Elaine Matthews
NASA Goddard Institute for Space Studies, New York, New York

Short title: CHARACTERIZATION OF THE VEGETATION BY SATELLITE OBSERVATIONS

Abstract. This study presents an evaluation and comparison of visible, near-infrared, passive and active microwave observations for vegetation characterization, on a global basis, for a year, with spatial resolution compatible with climatological studies (0.25°x0.25°). Visible and near-infrared observations along with the NDVI come from AVHRR. An atlas of monthly-mean microwave land surface emissivities between 19 and 85 GHz has been calculated from SSM/I observations for a year, suppressing the atmospheric contamination problems encountered with the use of simple channel combinations. The active microwave measurements are provided by the ERS-1 scatterometer backscattering coefficients at 5.25 GHz. The capacity to discriminate between vegetation types and to detect the vegetation phenology is assessed in the context of a vegetation classification obtained from in situ observations. A clustering technique derived from the *Kohonen* topological maps is used to merge the three data sets and interpret their relative variations with surface characteristics.

NDVI varies with vegetation density, but saturates for arid grassland and for forested areas. Spurious seasonal cycles and large spatial variability in several areas suggest that atmospheric contamination (cloud, water vapor, ozone, and aerosols) and/or solar zenith angle drift still modulate the NDVI signal. Passive and active microwave observations are primary sensitive to overall vegetation structure: They respond to absorption, emission and scattering by vegetation elements, including woody parts. Backscattering coefficients from ERS-1, measured with an accuracy of 5%, are not sensitive to atmospheric variations and exhibit good potential for vegetation discrimination with ~10 dB dynamic from rain forest to arid grassland. Passive microwave measurements also show some ability to characterize vegetation, but are less sensitive than active measurements. However, passive observations show sensitivity to the underlying surface wetness that enables detection of wetlands even in densely vegetated areas.

This study illustrates overall features of vegetation cover characterized by the

suite of data. Merging the data sets using clustering techniques capitalize on the complementary strengths of the instruments for vegetation discrimination and shows promising potential for land cover characterization on a global basis.

1. Introduction

Land cover physical characteristics are crucial boundary conditions for climate models that influence the exchanges of energy, water, and carbon between the biosphere and the atmosphere. Land surface parameterization for GCMs relies on global fields of terrestrial biophysical parameters estimated from land cover characterizations derived from in situ surveys [*Matthews*, 1983] or from vegetation indices calculated from satellite data in the visible and near-infrared [*Sellers et al.*, 1994; 1996]. The Normalized Difference Vegetation Index (NDVI) calculated from the red and near-infrared channels of the Advanced Very High Resolution Radiometer (AVHRR) has been extensively used for vegetation studies. The availability of the NDVI data for two decades and its high horizontal spatial resolution (up to 1 km) have motivated a large number of studies from regional to global scales [e. g. *Tucker*, 1985; *Myneni et al.*, 1998; *DeFries et al.*, 1999], relating NDVI to vegetation biophysical properties. However, there are growing concerns about the ability of the NDVI to quantitatively represent the vegetation properties and NDVI sensitivity to atmospheric factors and instrument calibration is debated [*Gutman*, 1999].

Lower resolution space-borne sensors operating in the microwave part of the spectrum have also shown some ability to characterize the land surface at spatial resolutions compatible with climatological applications. For global vegetation characterization, these instruments have, to date, triggered less interest than their visible and near-infrared counterparts.

Passive microwave observations from the Scanning Multichannel Microwave Radiometer (SMMR) on board NIMBUS 7 starting in 1978 and from the Special Sensor Microwave/Imager (SSM/I) on board DMSP satellites since 1987 have been used in vegetation studies, especially in conjunction with NDVI responses. Most studies have focused on the use of simple indices like the microwave vegetation index (MVI) which is based on the polarization difference at 37 GHz [e. g., *Choudhury and Tucker*, 1987;

Justice et al., 1989]. However, as noted by several authors [*Tucker*, 1989; *Kerr and Njoku*, 1993], atmospheric effects, especially cloud cover, is responsible for a large part of the 37 GHz polarization difference, casting doubt on the interpretation of simple indices solely in terms of surface properties. Recently, *Prigent et al.* [1997, 1998] calculated land surface microwave emissivities from SSM/I observations by removing contributions from the atmosphere, clouds and rain using ancillary satellite data. The results show promising correspondences between geographical and seasonal patterns of the emissivities and global land surface characteristics.

Multi-year active microwave data over the entire globe are a new resource available since July 1991 with the launch of the European Remote Sensing satellite ERS-1 carrying a wind scatterometer operating at 5.25 GHz (C-band). Scatterometers provide measurements of the backscattering coefficient of the observed surface. Primarily designed for estimating wind speed and direction over the ocean, space-borne scatterometers have also shown good correlation with vegetation dynamics at global and regional scales. Preliminary results were obtained with 3 months worth of data from the scatterometer on board Seasat-A in 1978 [*Kennett and Li*, 1989] and were later confirmed by several authors using ERS-1 and 2 data [*Kerr and Magnani*, 1993; *Wisman et al.*, 1993; *Frison and Mougin*, 1996 a, b].

The objective of this study is to compare the ability of these different measurements to characterize the spatial distribution of the vegetation and its phenology and to examine how complementary strengths of the instruments can be used to obtain maximum information about vegetation physical characteristics on a global basis. The three types of observations analyzed here cover a large portion of the electromagnetic spectrum: 1) AVHRR visible ($0.58 - 0.68\mu$m) and near-infrared ($0.73 - 1.1\mu$m) reflectances and the derived NDVI, 2) passive microwave SSM/I emissivities between 19 and 85 GHz (i. e. from 1.58 cm to 0.35 cm in wavelength), and 3) ERS-1 active instrument backscattering coefficient at 5.25 GHz (wavelength = 5.71 cm). Actually

our analysis of SSM/I also uses observations in the visible and infrared ($\sim 11\mu$m) to identify cloud-free scenes and measure surface skin temperatures, but in this study we do not consider the possible information about the land surface properties that may be obtained from temperature data.

A year of monthly-mean observations of each instrument is examined, at a spatial resolution of $0.25° \times 0.25°$. This spatial resolution was chosen to be appropriate for global climate studies. The three data sets are described in section 2. Section 3 briefly reviews the responses of each wavelength range to the land surface characteristics, as background in interpreting the monthly-mean distribution of the data sets. The ability of each instrument to discriminate among vegetation types and to capture the seasonal cycle is analyzed on a global basis (Section 4). The classification of vegetation by *Matthews* [1983] is used as a reference. A clustering technique stemming from *Kohonen* topological maps is implemented to merge the three data sets and to enable a synthetic analysis of the respective variations of the spectral bands (section 5). Section 6 concludes this study and suggests potential applications of the clustering technique for land cover classification.

2. The data sets

This study evaluates globally and routinely available satellite data for their potential for vegetation characterization with a spatial resolution compatible with climatological studies. A full annual cycle from July 1992 to June 1993 is analyzed. The three satellite data sets are mapped on an equal area grid of $0.25° \times 0.25°$ resolution at the equator and monthly-mean values are calculated from daily values.

High resolution data from visible and near-infrared (Landsat, Spot) or from synthetic aperture radar (SAR) have been investigated for local scale studies. However, because of the large volume of data associated with those high resolution observations and because of their incomplete coverage on a global and continuous basis, lower

resolution instruments are preferred for global scale studies.

The three satellite products are described in this section along with the *Matthews'* vegetation data set. This vegetation classification has been widely used and provides a test of the ability of the remote sensing instruments to distinguish among vegetation types.

2.1. Visible and near-infrared reflectances and NDVI from AVHRR

The AVHRR instruments on board the NOAA meteorological polar orbiters provide daily observations of the Earth with a spatial resolution of up to 1 km. The first AVHRR channel is in the visible VIS 0.58-0.68 μm) where chlorophyll causes absorption of incoming radiation and the second channel is in the near-infrared (NIR 0.73-1.1 μm). NDVI is calculated as the ratio of the difference of the AVHRR channels 2 and 1 over their sum.

Several AVHRR global data sets have been produced. Monthly AVHRR products at 8 km resolution are generated under the joint NASA and NOAA Earth Observing System Pathfinder project [*James and Kalluri*, 1994]. They are available at NASA GSFC Distributed Active Archived Center (WEB site http://gsfc.nasa.gov), along with a description of the data calibration and processing. Correction for Rayleigh scattering is performed, but there is no atmospheric correction for clouds, water vapor, aerosols, and ozone. However, NDVI composite maps correspond to the maximum value of the NDVI for the compositing time period, which tends to minimize atmospheric contamination [*Holben*, 1986]. Solar zenith angle dependences are related to both annual solar cycle and changes in the equator crossing time. They are not accounted for in the reflectances and can introduce a spurious seasonal variation in the NDVI signal that may be falsely attributed to vegetation changes [*Gutman*, 1999]. *Gutman* [1999] describes the data set in detail and analyzes its quality. He reviews instrument performance and satellite orbit characteristics. For NOAA 11, which covers the period

of this study, the anomalies in the channel 1 and 2 reflectances should be no more than $\pm 1\%$ and $\pm 2\%$, respectively [*Gutman*, 1999]. Using a simple error propagation equation, these errors translate into an accuracy of ~ 0.1 in the NDVI for typical values of the VIS and NIR reflectances. Several problems are mentioned (inter-sensor calibration, sensor degradation, satellite drift and changes in the solar zenith angle, contamination by clouds, water vapor, aerosols, and ozone) that hamper the interpretation of NDVI as vegetation only. From radiative transfer calculations, *Tucker et al.* [1992] carefully quantify the effect of atmospheric constituents in the VIS and NIR reflectances. Water vapor absorption essentially affects the NIR reflectances and depresses it by 10-30 % in sparsely vegetated areas. That translates into a decrease of up to 0.1 in the NDVI. Ozone can reduce the reflectance in channel 1 by 5-15% of its value. Aerosols can completely masks the vegetation properties with changes up to 0.2 in the NDVI in densely vegetated areas. *Gutman* [1999] draws attention to the NDVI problems and stresses that NDVI investigations, especially those directed at long-term trends, encounter serious challenges.

In this study, the VIS and NIR reflectances and the NDVI monthly-mean products are investigated. Data are averaged from their 8 km Pathfinder nominal resolution to an equal area grid of $0.25^\circ \times 0.25^\circ$ at the equator.

2.2. Microwave emissivities between 19 and 85 GHz (SSM/I)

The SSM/I instruments on board the DMSP polar orbiters observed the Earth twice-daily at 19.35, 22.235, 37.0 and 85.5 GHz with both vertical and horizontal polarizations, with the exception of 22 GHz which is vertical polarization only [*Hollinger et al.*, 1987]. The observing incident angle on the Earth is close to 53°, and the elliptical fields of view decrease in size proportionally with frequency, from 43x69 to 13x15 km^2. *Hollinger et al.* [1990] provide an evaluation of the instruments and inter-sensor calibration was examined by *Colton and Poe* [1999]. Pioneer investigations of the

sensitivity of passive microwave to vegetation used linear combinations of channels [e. g. *Choudhury and Tucker*, 1987] but these simple indices are contaminated by variations in atmospheric parameters and surface temperature. Microwave emissivities of land surfaces were recently estimated from SSM/I observations by removing contributions from the atmosphere, clouds, and rain using ancillary data from the International Satellite Cloud Climatology Project (ISCCP) [*Rossow and Schiffer*, 1991; *Rossow et al.*, 1996] and the National Centers for Environmental Prediction (NCEP analyses) [*Kalnay et al.*, 1996]. The method is fully described in *Prigent et al.* [1997, 1998], and summarized here. Cloud-free SSM/I observations are first isolated with the help of collocated visible/infrared satellite observations (ISCCP data). The cloud-free atmospheric contribution is then calculated from an estimate of the local atmospheric temperature-humidity profile from NCEP reanalysis. The atmospheric contribution varies from place to place and amounts up to 15% and 50% in the Tropics for 19 GHz and 85 GHz respectively. Finally, with the surface skin temperature derived from IR observations (ISCCP estimate), the surface emissivity is calculated for all the SSM/I channels. The standard deviation of the day-to-day variations of the retrieved emissivities within a month are typically 0.013 for all channels and for their polarization difference which is a measure of the precision of these estimates. Monthly-mean values are calculated with a spatial resolution of 0.25°.

2.3. Microwave backscattering at 5.25 GHz (ERS-1 scatterometer)

The European Space Agency (ESA) ERS wind scatterometer operates at 5.25 GHz vertical polarization with a 50 km spatial resolution. General characteristics and performance of the ERS scatterometer can be found in *Frison and Mougin* [1996 a]. The backscattering signal is continuously measured by three antennas, one looking normal to the satellite flight path and the other two pointing 45° forward and backward respectively. The instrument scans a 500 km wide swath with viewing

angles ranging from 18° to 59°. The ERS scatterometer shares some hardware with the synthetic aperture radar (SAR) and the SAR and the scatterometer modes are mutually exclusive. Therefore, over some areas where the SAR is typically on (North America, Europe), the temporal sampling rate for the scatterometer is lower. With the scatterometer operating continuously, global coverage would be achieved in about 4 days. The scatterometer response is very stable over time for non-changing targets and the measurement uncertainty is estimated to be about 5%. Water vapor and cloud absorption/emission are negligible at 5.25 GHz and no atmospheric correction is required for the scatterometer signal. *Frison and Mougin* [1996 a] show that the antenna inter-calibration is very good, which enables the use of all three antennas. They also demonstrate that azimuth angle effects are small over vegetated surfaces, although strong anisotropic signatures are observed over some deserts. For incidence angles between 25° and 50°, scatterometer responses can be approximated by a linear function of the incidence angle. *Frison and Mougin* [1996 b] compared the scatterometer responses at various incidence angles and showed that the radar signal at low incidence angles ($\leq 20°$) is related to soil characteristics whereas observations at large incidence angles ($\sim 45°$) provide more information about vegetation. In addition, radar signals at low incidence angles exhibit a larger scatter and a smaller dynamic range within a year. Other studies [e. g. *Wagner et al.*, 1999 a] suggest fitting a model to the slope of the angular dependence at 40° because this parameter is supposed to be less sensitive to the soil moisture. However, this parameter is very sensitive to noise and several years of data are required to calculate it.

Following the method developed by *Frison and Mougin* [1996 a] for each cell on an equal area grid of 0.25°x0.25° at the equator, a linear fit is calculated for all incidence angles between 25° and 50° for a month and the fitted value at 45° is kept.

2.4. Matthews' vegetation classification

Matthews' vegetation and land-use data set was compiled from a large number of published sources [*Matthews*, 1983]. At a 1° spatial resolution, the vegetation classification distinguishes a large number of vegetation types, typically grouped to 30 classes of natural vegetation. Associated with the vegetation classification is a land-use data set that distinguishes five levels of cultivation intensity, ranging from 0 to 100% cultivation. Combining the vegetation and land-use data set gives information about actual land cover. Table 1 presents *Matthews'* vegetation classification for the 30-vegetation classes along with a simplified 9-class grouping on the basis of life form. For each vegetation class, areas with cultivation intensity of $\geq$ 50% are defined as cultivation which makes up a tenth class. The vegetation classes are indicated by Vn for the 10-class and by vn for the 31-class classification.

3. Brief review of the different wavelength responses to surface characteristics and presentation of monthly-mean maps

3.1. Visible, near-infrared reflectances and the NDVI

Green vegetation exhibits a characteristic reflectance curve. Snow-free reflectance is $\sim$ 0.05 in the VIS portion of the spectrum ($\leq$0.7 μm) with a steep rise in the NIR (0.7-1.1 μm) to about 0.20. Seasonally, the rise of full-spectrum albedo from the beginning to the peak of the growing season is the net effect of two opposing trends [*Bauer and Dutton*, 1962; *Pinty and Szejwach*, 1985]. The spring-summer increase is governed by declining reflectance in the VIS and increasing reflectance in the NIR. Full-spectrum albedo declines from the growing season maximum to some lower autumn value through a reversal of the VIS and NIR trends. These seasonal variations result in a NIR/VIS ratio that increases during the growing season and declines abruptly

at the end of the growing season. The growing-season minimum in the VIS is due primarily to chlorophyll absorption at ~0.65 μm [*Knipling*, 1970]. Individual leaves do not absorb NIR radiation significantly and NIR reflectance of vegetation canopy is due to complex interactions within the internal leaf structure and between the leaves, the canopy structure, and the soil background [*Scott et al.*, 1968; *Knipling*, 1970; *Sinclair et al.*, 1971; *Gausman*, 1974]. *Colwell* [1974] insists on the important role of vegetation structure, soil reflectance, and observation geometry (especially solar zenith angle) in understanding and predicting vegetation canopy from NDVI. From ground-based measurements, several authors have mentioned the difficulty of differentiating between vegetation types from reflectances only [*Scott et al.*, 1968; *Sinclair et al.*, 1971] and they suggest exploring the temporal changes of the reflectances. *Tucker* [1979] showed correlation between the properties of the vegetation canopy and the reflectances (in the VIS at 0.65 μm and in the NIR), while *Scott et al.* [1968] only observed such a correlation in the VIS.

Different combinations of the reflectances in the VIS at 0.65 μm and the NIR have been investigated [e. g. *Tucker*, 1979; *Begue and Myneni*, 1996]. They are all sensitive to the presence of vegetation but are differently affected by changes in soil color and brightness. NDVI is the most widely used. It capitalizes on the magnitude of reflectance differences between spectral bands and on its seasonal variations.

NDVI has been found to be correlated with the fraction of photosynthetically active radiation (FPAR) absorbed by green vegetation (since it is related to spectral albedo), to leaf area index (LAI) [e. g. *Asrar et al.*, 1984; *Begue and Myneni*, 1996], and to carbon fixation [*Fung et al.*, 1987], as well as providing information about vegetation phenology [*Moulin et al.*, 1997].

3.2. Passive and active microwave responses over land

Microwave responses of the land surface include contributions from the vegetation and from the underlying surface. An extensive body of research has been directed toward a better understanding of the mechanisms responsible for the microwave emission and backscattering of soil and vegetation, both from theoretical analysis and from small-scale field experiments using hand-held, truck-mounted, or airborne sensors. A review of these studies is presented by *Ulaby et al.* [1986] and more recent developments include modeling by *Karam et al.* [1995], *Wigneron et al.* [1993], *Ferrazzoli and Guerriero* [1996] or measurements by *Matzler* [1990], *Wigneron et al.* [1997], *Hewison* [2000].

Vegetation absorbs, emits and scatters microwave radiation. Radiative properties of vegetation are mainly driven by the dielectric properties of the vegetation components, their density, and the relative size of vegetation components with respect to the wavelength. Dielectric properties of vegetation are closely related to their water content. Increasing vegetation density usually reduces the emissivity polarization difference [*Choudhury*, 1989] and increases the backscattered signal [*Mougin and Frison*, 1996 a]. Both theory and in situ measurements predict increasing absorption/emission and scattering by vegetation with increasing frequency, and as a consequence the underlying surface contribution is expected to increase with decreasing frequency.

Bare soil response depends on soil dielectric properties and roughness. At satellite resolution, smooth bare soils have a quasi-specular reflection, producing high polarization emissivity differences around 50° incidence and low backscattering coefficient. When the terrain gets rougher, surface scattering causes the emissivity polarization difference to decrease and the backscattering coefficient to increase. In dry soil, volume scattering can be involved producing low radar return [*Deroin et al.*, 1997] and specific passive microwave signatures [*Prigent et al.*, 1999].

Water has a high dielectric constant compared to bare soil. For passive measurements, open water surfaces (lakes, inundated areas) exhibit very low emissivities

in both horizontal and vertical polarizations along with a high polarization difference. Passive microwave measurements can be used to detect inundation [*Gidding and Choudhury*, 1989; *Sippel et al.*, 1998]. Active instruments measure low backscattering coefficients over water surfaces. Microwave emissivities and backscattering coefficients are also sensitive to soil moisture. Recent investigations includes studies by *Owe et al.* [1999] and *Vinnikov et al.* [1999] for passive microwaves and by *Wagner et al.* [1999 b] for the active measurements. However, soil roughness and presence of vegetation are serious challenges for the detection of soil moisture variations. While several in situ measurements of land surface emissivities and backscattering coefficients have been conducted, they do not cover the large diversity of surface types on the globe and extrapolation from small scale measurements to satellite field of view is not trivial.

3.3. Presentation of monthly-mean maps

Figure 1 presents monthly-mean values of NDVI (AVHRR), emissivity polarization differences at 37 GHz (SSM/I), and scatterometer backscattering coefficients at 5.25 GHz (ERS-1) for August 1992, along with the vegetation classification map for 10 classes. There are qualitative correspondences between the three types of observations and the vegetation classification.

Desert areas (V9) are characterized by low NDVI, large emissivity differences and low backscattering coefficients, and are clearly noticeable on each map. Variations of the backscattering coefficients and the emissivities over desert areas are interpreted in terms of rock/sand types and topography. Higher values of backscattering and lower values of emissivity polarization differences are found over high topography in the desert (Tibesti, Air in the Sahara).

Tropical rain forests display large backscattering coefficients and negligible emissivity polarization differences. However, the tropical rain forest in Africa shows rather low NDVI values compared to the rain forest in South America. Grassland and

woodland can also be distinguished in Africa and in South America. The sharp gradient southward of 15°N in Africa is observable on all the maps: it corresponds to the Sahelian transition between arid shrub grassland and more humid grassland with tree cover.

Water surfaces (lakes, rivers, wetlands) show high emissivity polarization differences at 37 GHz. The major river systems (e. g. Congo, Amazon) and wetlands (e. g. Pantanal in South America) appear clearly on the microwave emissivity map while they are not easily detectable on the NDVI or on the backscattering coefficient maps. With the ERS-1 scatterometer working at 5.25 GHz, one would expect less absorption by vegetation at 5.25 GHz ERS-1 frequency than at SSM/I higher frequencies and a stronger contribution from the underlying surface. The opposite is observed.

4. Evaluation of the potential of the satellite data sets for vegetation monitoring

4.1. Ability to distinguish major vegetation classes

Figure 2 represents the histograms of the different observations for 4 major vegetation types in areas in the northern hemisphere where the cultivation intensity is $\leq$20%. Evergreen and deciduous forests have been grouped together because during summer months no significant differences are observed; the same is done for woodland. The analysis is not restricted to the parameters that are commonly investigated for vegetation studies (NDVI, emissivity polarization differences) but also includes an examination of the individual channel responses. For a given observation, the histograms are normalized to have the same area, giving an estimate of the probability distribution function.

For AVHRR, from separate channel information (VIS or NIR), only two classes of vegetation appear to be distinguishable and even these have substantial overlap in reflectance distributions. Absorption by chlorophyll decreases with the amount of active

photosynthetic parts in the vegetation and as expected the visible reflectance is lower for grassland than for woodland and forest. Lower reflectances could also be interpreted in terms of larger fractional coverage by bare soils which have higher VIS reflectances. There is more variability in the NIR than in the VIS. Both the VIS and the NIR signals saturate for higher biomass density: It is not possible to distinguish between woodland, forest and rain forest, based simply on a month's data. Combining those two pieces of information in the NDVI helps differentiate woodland from forest, but rain forest and other forests still appear very similar. Other authors also observed saturation of the NDVI response for high green-leaf density [e. g. *Tucker*, 1985]. There are two peaks in the woodland histogram for the NDVI (also seen on the VIS histogram) with the lower value peak corresponding to arid East Africa.

For SSM/I, vegetation information is similar at all frequencies. Separating vegetation via individual SSM/I channels (vertical or horizontal polarization) cannot be done. The emissivity in horizontal polarization is lower for grassland than for tree-covered areas. With decreasing vegetation density, the contribution of bare soil surfaces within a pixel increases, reducing emissivity in the horizontal polarization. The emissivity in vertical polarization shows little variation: Emissivities are slightly smaller for rain forest than for other forested regions, which may be explained by the large water volume in big leaves inducing significant scattering. However, given the absence of in situ radiometric measurements over rain forest, this hypothesis cannot be confirmed. Calculating the emissivity polarization difference helps separate rain forest from other forest/woodland and from grassland. Nevertheless, discrimination between forest and woodland is not possible.

With increasing vegetation biomass, the backscattering signal from ERS-1 increases and the four histograms are rather well separated, except for grassland and with overlapping between forest and woodland. Given the estimated error of 5%, a $\sim$4 dB range between the peaks of tree-covered classes represents a significant vegetation signal

that is promising for discrimination of vegetation density gradients. The grassland backscatter histogram is wide as it is for all other observations (except for the emissivity in vertical polarization). It even has two peaks in the NDVI: the peak with high NDVI values corresponds well to grassland with partial tree cover, while the other peak is related to locations with less woody cover (see the 31-class vegetation classification in Table 1). By the same token, forest and woodland classes may also contain partial coverage by grassland, which might explain the difficulty of separating the grassland and the woodland/forest classes.

Similar results are obtained in the southern hemisphere, but with more confusion between forest and woodland.

4.2. Ability to detect the vegetation phenology

For the different observations in the northern hemisphere, Figure 3 shows the histograms for 6 vegetation types for three months that correspond to different vegetation stages. Areas where the cultivation intensity is larger than 20% are excluded as are pixels that are snow-covered for at least one of the three months. The snow cover information comes from the NOAA operational analysis. The mean difference between August 1992 and February 1993 is indicated, along with its standard deviation.

Rain forests have a stable signature in time for both passive and active microwave observations; this stability is clear for all months. NDVI responses over rain forest are unstable, especially in the southern hemisphere (not shown). That has also been observed by *Tucker et al.* [1985] over Africa and they explain their findings by the specific ecology of the rain forest in Africa compared to the other rain forests elsewhere. However, the variations in Figure 3 can more probably be attributed to contamination by atmospheric features such as water vapor and clouds. *Gutman* [1999] argues that over rain forest, the NDVI decreases with local zenith angle, driven by a decrease in the NIR due to water vapor absorption. High frequency of cirrus contamination over the

Tropics is also likely to induce spurious NDVI variability. Figure 4 presents scatterplots of VIS and NIR reflectances, NDVI, and radar backscattering versus the high cloud amount from ISCCP, for 6° × 6° area in the African rain forest (3S 3N; 17E 23E) and for a year. NDVI and VIS reflectances show unexpectedly large variances over the year that are linearly correlated to the amount of high clouds. No such correlation is found with the NIR and the radar signal, ruling out a possible correlation between high cloud amount and vegetation characteristics.

With microwave measurements (emissivity polarization differences and the radar backscattering), the responses are more stable throughout the year for evergreen forests (V3) than for deciduous ones (V2). In tree-covered regions, the emissivity polarization difference stays low even in winter and backscattering coefficient remains high. Interaction between the microwave signal and the vegetation is not limited to green leaves in the canopy but includes scattering and emission/absorption by woody parts comprising the structure of the canopy; these results suggest that the leaf contribution is relatively small. NDVI or individual VIS and NIR channels do not distinguish the two forest types: The differences in the histograms between months are about the same for the deciduous and the evergreen forest, and surprisingly, the deciduous forest has the same signature in August and December.

Especially for grasslands, variations in the NDVI are essentially due to variations in the NIR and not in the VIS. Changes in the VIS channel are small over the year and are of the order of the measurement noise. For the NIR, seasonal changes are larger, but they have similar range for all vegetation types except rainforest. As discussed by *Gutman* [1999], solar zenith angle variations can be partly responsible for the seasonal cycle of the reflectances. Water vapor variations can also modulate the signals. *Justice et al.* [1991] observed that water vapor absorption in the NIR channel may drive part of the NDVI seasonal variation, especially over grassland. *Tanre et al.* [1992] show that for grassland over Mali, correcting the NDVI from water vapor contamination can

increase it by 0.1 for wet days. C. Brest at NASA Goddard Institute for Space Studies at GISS (personal communication) also performed a water vapor correction to AVHRR data and observed a change of ~0.05 in reflectances over tropical areas. Water vapor induced change in the NDVI is modulated by the water vapor amount, the geometry of the observation and the surface reflectance itself: simple correction of the NDVI values cannot be easily implemented and a full treatment of the water vapor absorption is a requirement for an adequate interpretation of the reflectances in terms of surface properties only.

Individual passive microwave channels are not able to capture the seasonal cycle of any vegetation type and mean differences between maximum and minimum in the vegetation cycle is within the noise level ($\sim$ 0.013). However, both the emissivity polarization difference and the backscattering coefficient show realistic variations within the year that can be attributed to vegetation seasonality, although the magnitude of the microwave seasonal response is small, especially for the passive measurements.

4.3. Ability to distinguish between vegetation subclasses

The subdivisions of forests and woodlands (see Table 1) are essentially driven by climate zone and as a consequence, differences in the signals are not expected from for instance tropical and temperate evergreen needle-leave forests. That has been verified but is not shown here.

Separability between broad-leaved and needle-leaved tree-covered areas is very difficult to assess because the two leaf types exist in different climate regions. For instance, evergreen broad-leaved woodland (v13) is concentrated in coastal regions in Australia while evergreen needle-leaved woodland dominates in Canada above 50°N. Attributing small signature differences exclusively to leaf type is misleading, given the large climatological differences between the two regions.

The grassland subclasses (classes 23 to 29 in the 31-class classification) present

different biomass densities that should have different signatures in the observations. Figure 5 shows time series of three grassland types v23 to v25 which represent grassland with decreasing tree cover, in the two hemispheres (see Table 1). With decreasing woody coverage, the biomass density is lower and one expects to observe: 1) increasing values of the polarization emissivities for passive microwave, 2) reduced backscattering signal for radar, and 3) lower NDVI values especially during summer months. In the southern hemisphere, these patterns are apparent but in the northern hemisphere, differences between v23 and v24 are opposite to what is expected with all instruments. In this case, the vegetation classification may be questioned. Differences between classes 26 to 28 are related to grassland height from tall to short grassland, which should correspond to decreasing vegetation density: The expected responses are observed with the various measurements (not shown), but with a lot of scatter. The vegetation classification may have to be revisited in the light of these satellite measurements, especially in South America and Africa where land use practices may not be well documented and where anthropogenic modification of the vegetation on short time scales is occurring.

4.4. A case study: The desert/rain forest transition in Africa

Values of NDVI, ERS-1 backscattering and SSM/I emissivity polarization differences (Figure 6) are compared for August and February along a cross-section at longitude 20E that encompasses a strong north-south gradient of vegetation, from the desert in Chad (latitude 20N) to the rain forest in the Democratic Republic of Congo (latitude 0N). In this region, the vegetation phenology is driven by rainfall, with an increase in the rainy season duration and in the amount of precipitation from north to south. For specific sites along the cross section, the annual cycle of the three observations are presented along with the precipitation cycle as given by the Global Precipitation Climatology Project from merged infrared and microwave satellite data and gauge measurements [*Huffman et al.*, 1996]. The vegetation type is indicated as given by *Matthews*' 31-type

classification. All the variables are normalized for an easier comparison (see the figure caption).

North of 16N, the three observations are stable in time, with low NDVI values and high emissivity polarization differences. The backscattering signatures change abruptly between 17N and 18N: Around 17N, sand dunes induce a very low backscattering signature because of volume scattering in sand, while north of 18N, the backscattering signal increases with the presence of rocks [*FAO-UNESCO*, 1977].

South of 16N, variations between summer and winter increase for all observations. From (16N,20E) to (6N, 20E), the seasonal cycle of the various grassland types (from classes 23 to 25) is well captured by the three types of observations, and the observations are varying in phase. The vegetation growth is associated with the rainy season, with a rapid vegetation development as soon as the rainy season starts, and a slow decrease in the senescence phase. *Frison and Mougin* [1998] analyzed the respective contributions of the soil and vegetation in a case study in a semi-arid environment in Northern Sahel (Mali), concluding that although the soil component is always large, the backscattering coefficient reflects the vegetation development well. As expected, passive and active microwave responses are very stable in the rain forest (see the annual cycle at 1N, 20E). However, for the same area, NDVI exhibits large variations during the year that cannot be explained in terms of vegetation.

At specific locations along the cross-section, the SSM/I response shows large increases in the emissivity polarization differences especially in August during the rainy season. At 10N for instance, the decrease in the emissivity polarization differences is related to the Slamat swamps in Chad. The decrease around 13N could be related to swamps around the Batha river in Chad, but that should be further investigated. Around 2N in the rain forest, the Congo river and its associated swamps induce a decrease in the emissivity polarization. There are no significant changes in the backscattering coefficient nor in the NDVI.

4.5. Correlation between the three types of observations

Figure 7 represents the scatterplot of all possible pairs of observations, for the NDVI, the backscattering coefficient, and the emissivity polarization difference at 37 GHz, for four major vegetation types in South America in August. For each scatter plot, the population contours at 0.2 and 0.5% are drawn.

For the rain forest, the ERS backscattering coefficients show little dispersion, while the NDVI and the emissivity polarization difference exhibit larger scatter. For the NDVI, atmospheric contaminations are suspected. Pixels that have large emissivity polarization differences ($\geq$.01) are co ıcentrated in coastal areas an l around the major river systems (Congo in Africa, the Amazon in South America). Tl is confirms the high sensitivity of the passive microwave measurements to water surfaces, compared to the other measurements. Compared to the SSM/I responses, ERS-1 backscattering signal shows more dynamic range in densely vegetated areas outside wet areas, with population contours elongated along the backscattering coefficient axis. For emissivity polarization differences between 0.00 and 0.02, ERS backscattering coefficient varies from $\sim$-7 dB to $\sim$-12 dB over forest and woodland with lower values of the backscattering coefficients corresponding to the transition zones between forest/woodland and grasslands. ERS-1 radar signal has the ability to detect density gradients in forested areas. For grasslands, the backscattering signal and the SSM/I response are almost linearly related, but this is not true for NDVI. NDVI signal shows a large dynamic for low emissivity polarization differences and for rather high radar signals, while the NDVI reaches saturation for high emissivity polarization and for low radar signals. Similar behavior has been observed by *Becker and Choudhury* [1988], *Tucker* [1989], among others. Over sparsely vegetated areas, the large variability of the microwave signals are explained by their sensitivity to bare soil roughness and moisture. Given that all vegetation types show a large NDVI variability, it is difficult to attribute the large dynamic of the NDVI to vegetation changes alone: It can also be related to atmospheric contamination of the signal.

5. Merged analysis of spectral variations with clustering technique

5.1. Description of the clustering technique

In the preceding sections, we analyzed the response of individual spectral band to a given type of vegetation. We also examined relations between pairs of spectral bands. A clustering technique has been developed to merge all the data sets to obtain an analysis of the variations of one spectral band with respect to the others. At this stage, the clustering technique is a tool to help interpret the variability of the channels; it is not yet optimized for vegetation classification.

Let $\{X^i \in R^n \ ; \ i = 1, \ldots, M\}$ be an observation dataset, where n is the dimension of the observation (i.e. the number of channels in the following) and M the number of observations (i.e. the number of monthly-mean pixels in the following). The goal of unsupervised classification algorithms is to classify this data set into subgroups that optimally describe the statistical variability present in the data, without any *a priori* information about actual physical classes. Clustering techniques define K prototypes (or clusters) P^i that give a discrete description of the continuous observations and optimally quantify their variability. Each observation X^i is associated with the prototype for which the distance $d(X^i, P^k)$ is the smallest.

Kohonen topological feature maps are also called self-organizing topological maps [*Kohonen*, 1982]. The specificity of this algorithm compared to other clustering techniques is obtained by imposing a neighborhood requirement on the prototypes. When the algorithm has converged, prototypes corresponding to nearby points on the feature map grid also have nearby locations in the data space. This additional information on the extracted prototypes makes it easier to interpret each prototype. The neighborhood system adopted in this study is a one dimensional ordering of prototypes where the neighborhood of a prototype is its two nearest neighbor prototypes. This

neighborhood system is well adapted to the definition of a statistical index that is a particularly good way to describe the links and the variabilities in the dataset.

The *Kohonen* classification algorithm is applied to a year of monthly-mean observations for SSM/I, ERS-1, and AVHRR (M=12). Each observation vector corresponds to one snow-free pixel of 0.25° × 0.25° has 13 components (n=13) which are 1) 9 SSM/I derived variables: the emissivities for each polarization and their polarization difference at 19, 37 and 85 GHz, 2) the ERS-1 backscattering coefficient, and 3) the AVHRR reflectances in the VIS and NIR and the NDVI. Each observation in the observation vector is normalized by its mean spatial variance over a year. The same weight is given to each instrument, meaning that each individual observation is weighted by a coefficient 1/9 for SSM/I and 1/3 for AVHRR. The number of prototypes K is chosen to be 30. The distance d is the absolute value of the difference; compared to the traditional Euclidien distance, it gives less weight to potential outliers.

5.2. Results of the clustering and joint analysis of the spectral bands

The *Kohonen* algorithm is applied to estimate the $K = 30$ clusters, P^k, that optimally quantify the dataset. After the convergence of the algorithm, each observation X^i is associated with its closest prototype using the distance d. A cluster map is produced for each individual month; Figure 8 shows the results for August 1992. Figure 9 represents the $n = 13$ coordinate values (i.e. the channel observations) of each prototype P^k with respect to the cluster number, from cluster 1 to cluster $K = 30$. The standard deviation of the subgroup of observations associated with each prototype is added to the figure. For a given prototype, a low standard-deviation in one channel means that the channel provides good discriminant information in the clustering solution: the relation between the cluster and the channel is not ambiguous. On the other hand, a high standard-deviation means that the prototype is relatively insensitive to the particular channel. Such a high standard deviation could originate

from instrumental noise or from additional variability that contaminates the channel and is not related to the surface properties (atmosphere contamination for example).

The number of prototypes K has been chosen so that, for each consecutive prototypes, at least one of the channel is sufficiently statistically discriminant: For this channel, the difference between the two prototypes is above the standard-deviation of subgroups associated with each prototype. The ambiguity between prototypes is thus limited. As a consequence, on the map, each class shows a good spatial consistency. The variability of each cluster subgroup, which depends on the value and the number of observations in the subgroup, has been uniformly distributed by the *Kohonen* algorithm in each prototype for an optimal quantification of the dataset.

The 30 clusters have been separated into three contiguous groups (see Figure 8). The three groups can be associated with arid environments (clusters 1 to 10), vegetated areas (clusters 11 to 24) and wet regions (clusters 25 to 30). Clusters 11 to 24 can be compared to a vegetation density gradient that shows similarities with *Matthews'* vegetation classification. Although it is not our purpose here to classify the vegetation, a quick comparison is performed between the clustering results and *Matthews'* classification for the northern hemisphere in August. 58% of class V1 in *Matthews'* classification correspond to cluster 24, and 17% are in cluster 25. Forest type (V2+V3) has its maximum population in cluster 21, while woodland (V4+V5) has it for cluster 19.

5.2.1. Arid environments. Clusters 1 to 3 correspond closely to sandy deserts [*FAO-UNESCO*, 1977] with high reflectances in the VIS and NIR, low backscattering signals from ERS-1 and large polarization differences for SSM/I. Clusters 4 to 8 have similar VIS and NIR reflectances, while the backscattering signal increases by ~9 dB due to increasing surface roughness related to the combined effects of rocky surfaces and topography. SSM/I polarization differences also decrease with surface roughness. Clusters 9 and 10 correspond to desert areas in high topography and they show a large

backscattering signal compared to the surrounding areas. Radar signals have a high sensitivity to surface roughness that could be used to characterize desert properties, especially in the context of estimating dust sources [*Marticorena et al.*, 1997].

5.2.2. Vegetated areas. The cluster numbers between 11 and 24 could be linearly transformed into a multivariate-source index related to vegetation density. Clusters 11 to 13 are predominantly located in arid areas. From cluster 14 to 24, NDVI, radar backscattering, and the microwave polarization differences show a smooth increase corresponding to increasing vegetation density. Changes in the backscattering signal amount to 6 dB, which is very significant compared to the 5% accuracy of the measurement. The backscattering standard deviation is very low for these clusters, indicating that the radar signal is the most effective discriminant factor. Although NDVI increases smoothly, its large standard deviation in these clusters shows that separation between clusters is not related to its value. NIR does not vary much while VIS reflectance changes from 0.15 to 0.05. In vegetated areas, emissivities in the vertical polarization decrease with increasing frequency, which is contrary to what models predict. This has already been observed and discussed [*Prigent et al.*, 2000]. For the horizontal polarization, the emissivities are almost constant except for very densely vegetated areas. These results reinforce the hypothesis of stronger scattering by vegetation with scattering increasing with frequency. These signatures will be further explored with the help of a radiative transfer model [*Wigneron et al.*, 1993].

5.2.3. Wet areas. From cluster 25 to 30, the passive microwave signals vary drastically with rather low standard deviation while the other variables show smaller changes with large standard deviations. This confirms the high sensitivity of the microwave signals to the presence of water and its potential for the detection of inundated areas. Figure 10 shows the response of the three instruments in the rain forest over the Amazon for a year. While the passive microwave clearly detects the wetland surrounding the river and its seasonal cycle, the active microwave instrument only

responds to scattering by the vegetation. With increasing frequency, one expects higher attenuation and scattering by vegetation and as a consequence a lower sensitivity to soil properties. Although operating at a lower frequency, ERS-1 scatterometer observations show much less sensitivity to the presence of inundated areas. This suggests that scattering by the vegetation could dominate the radiative transfer processes in the canopy, exceeding the absorption/emission contribution within the vegetation. Unified radiative transfer models are now capable of simulating both the emissivity and the backscattering responses of vegetation and soil [*Wigneron et al.*, 1993; *Karam et al.*, 1995]. Using radiative transfer model at 1.5 GHz, *Du et al.* [2000] attempt to assess which of the two sensing techniques (passive or active) is less affected by vegetation cover when trying to estimate soil moisture. They conclude that the two sensor types have similar sensitivity to vegetation. Joint analysis of the emissivity and backscattering model responses, compared to ERS and SSM/I observations, will help better understand the vegetation and soil interaction with the microwave radiation.

6. Conclusion

This study presents a global evaluation and comparison of measurements in the visible and near-infrared, as well as passive and active microwave for characterizing vegetation cover and seasonality. It is the first step toward a characterization of the land surface using multi-satellite observations covering a large spectral range. A year of monthly-mean observations of AVHRR (NDVI, visible and near-infrared reflectances), SSM/I (emissivities between 19 and 85 GHz) and ERS-1 (wind scatterometer backscattering coefficients) was analyzed at a $0.25° \times 0.25°$ spatial resolution which is compatible with climatological studies. The capacity to discriminate various vegetation types is assessed in the context of the *Matthews*' vegetation classification, with special emphasis on the ability to detect the vegetation phenology. A clustering technique derived from the *Kohonen* topological maps is developed to merge observations from all

three instruments and to provide a synthesis of the respective sensitivities of the various spectral bands to surface properties.

NDVI varies with vegetation density from ~ 0.1 to ~ 0.7 with an estimated error of 0.1 and saturates for forested areas. NDVI has a marked seasonal cycle for most vegetation types that is mostly driven by changes in the near-infrared reflectances, not by variations in the visible reflectances. Time series over evergreen vegetation show spurious seasonal variations of up to 0.2 in the NDVI. Significant cirrus contamination is evidenced over the African tropical forest. Atmospheric contamination (clouds, water vapor, aerosols, and ozone) and solar zenith angle dependences also alter the signal. A full correction of the VIS and NIR reflectances for atmospheric contamination is a requirement in order to interpret the signals in terms of vegetation only. This task has been undertaken at NASA GISS. Understanding spatial and temporal variations in the VIS and NIR reflectances is of primary importance for the interpretation and prediction of the surface albedo, which is a key parameter in the Earth energy budget.

Passive and active microwave observations respond to the absorption/emission and scattering by vegetation elements including woody parts; they are not directly sensitive to the green-leaf activity.

Active microwave backscattering observations (ERS-1) are not affected by variations in atmospheric conditions and do not require significant preprocessing. Measured with an accuracy of 5%, backscattering signals exhibit a high potential to characterize bulk vegetation density including green-leaf and woody structures with $\sim$10 dB changes from rain forest to arid grassland. In contrast to NDVI, they have a stable seasonal response over evergreen vegetation and show a realistic annual cycle over deciduous vegetation. In arid places, backscattering measurements are very sensitive to surface roughness and show very strong signatures over sand dunes, making them a potential tool for desert studies. Unaffected by atmospheric variability, scatterometers appear to be very promising instruments for land surface characterization, for their high sensitivity

to vegetation, and for their potential for desert investigations.

An atlas of microwave emissivities between 19 and 85 GHz has been calculated from SSM/I using ancillary data to remove atmospheric contributions. The resulting emissivity polarization differences show some ability to characterize vegetation types but with a smaller dynamic range than ERS-1 observations; values range from $\sim$ 0.00 for tropical forests to $\sim$0.08 for arid grasslands, with an estimated error of $\sim$0.013. Vegetation discrimination is not possible from individual polarizations and sensitivity to vegetation does not vary significantly with frequency. However, passive microwave measurements exhibit a strong sensitivity to standing water, making it possible to detect wetlands even in densely vegetated areas. A method to detect the inundated areas and their extent is under development, using both passive and active microwave instruments, with the active observations helping in the estimation of the attenuation by the vegetation. Although operating at a lower frequency, ERS-1 scatterometer observations show much less sensitivity to inundated areas. This suggests that scattering by the vegetation may dominate the radiative transfer processes in the canopy, exceeding the absorption/emission contribution within the vegetation. Unified radiative transfer models are now capable of simulating both the emissivity and the backscattering responses of vegetation and soil [*Wigneron et al.*, 1993; *Karam et al.*, 1995]. Joint analysis of the emissivity and backscattering model responses, compared to ERS and SSM/I observations, will help better understand the vegetation interaction with the microwave radiation.

Matthews' vegetation classification has been used as a reference in this analysis and it appears that this classification should be revisited in the light of this study, especially in transition zones and in semi-arid environments. *DeFries et al.* [1995] reviewed the dominant biophysical processes and concluded that among the most important vegetation characteristics controlling biospheric fluxes are growth form (tree, shrub, herb) and seasonality of woody vegetation (deciduous, evergreen). Our study

suggests that a combined analysis of observations from the three instruments may have the ability to characterize large-scale features of these two vegetation properties. Unsupervised clustering techniques using *Kohonen* topological maps helped the joint interpretation of the various spectral bands but also showed potential for land cover classification. From this sensitivity analysis, an optimal set of variables can be selected that are relevant for land cover characterization and a land cover classification can be performed. Further improvements of the clustering technique will include the use of observation time series for a year instead of monthly data in order to take into account the seasonal cycle of each vegetation type and the use of a priori information (altitude, latitude). Combining observations from the three instruments will make it possible to benefit from their complementary strengths to extract maximum information about vegetation biophysical characteristics on a global basis. It will also minimize problems related to one instrument only and should show a better potential to monitor change over time from series of benchmark behaviors derived from the suite of instruments.

Acknowledgment. This work is supported by NASA Mission to Planet Earth program. The ERS data have been provided by the European Space Agency and the CESBIO, Toulouse, France. We gratefully acknowledge the help of Pierre-Louis Frison (IFG, Marne-la-Vallee, France) and Eric Mougin (CESBIO, Toulouse, France) with the ERS-1 data analysis and interpretation. We would like to thank Christopher Brest (NASA/GISS) for fruitful discussions about the visible and near-infrared reflectances. We are also very grateful to Mathew Rothstein (NASA/GISS) for his help in processing the SSM/I and ISCCP data sets.

References

Asrar, G., M. Fuchs, E. T. Kanemasu, and J. L. Hatfield, Estimating absorbed photosynthetic radiation and leaf area index from spectral reflectance in wheat, *Agron. J.*, 76, 300-306, 1984.

Bauer, K. G. and J. A. Dutton, Albedo variations measured from an airplane over several types of surface, *J. Geophys. Res.*, 67, 2367-2376, 1962.

Becker, F., and B. J. Choudhury, Relative sensitivity of normalized vegetation index (NDVI) and microwave polarization difference index for vegetation and desertification monitoring, *Remote Sensing of the Environment*, 24, 297-311, 1988.

Begue, A., and R. Myneni, Operational relationships between NOAA-advanced very high resolution radiometer vegetation indices and daily fraction of absorbed photosynthetically active radiation, established for Sahelian vegetation canopies, *J. Geophys. Res.*, 101, 21275-21289, 1996

Choudhury, B. J., and C. J. Tucker, Monitoring global vegetation using Nimbus-7 37GHz data. Some empirical relations, *International Journal of Remote Sensing*, 8, 1085-1090, 1987.

Choudhury, B. J., Monitoring global land surface using Nimbus-7 37GHz data. Theory and examples, *International Journal of Remote Sensing*, 10, 1579-1605, 1989.

Colton, M. C., and G. A. Poe, Intersensor calibration of DMSP SSM/I's: F-8 to F-14, 1987-1997, *IEEE Transaction on Geoscience and Remote Sensing*, 37, 418-439, 1999.

Colwell, J. E., Vegetation canopy reflectance, *Remote Sensing of the Environment*, 3, 175-183, 1974.

DeFries, R. S. et al., Mapping the land surface for global atmospheric-biosphere models: Toward continuous distributions of vegetation's functional properties, *J. Geophys. Res.*, 100, 20867-20882, 1995.

DeFries, R. S., J. R. G. Townshend, and M. C. Hansen, Continuous fields of vegetation characteristics at the global scale at 1-km resolution, *J. Geophys. Res.*, 104, 16911-16923, 1999.

Deroin, J. P., A. Company, and A. Simonin, An empirical model for interpreting the

relationship between backscattering and arid land surface roughness as seen with SAR. *IEEE Transaction on Geoscience and Remote Sensing*, 35, 86-92, 1997.

Du, Y., F. T. Ulaby, and G. Dobson, Sensitivity to soil moisture by active and passive microwave sensors, *IEEE Transaction on Geoscience and Remote Sensing*, 38, 105-114, 2000.

FAO-UNESCO, Soil map of the world, 1:5M scale, UNESCO, Paris, 1977.

Ferrazzoli, P., and L. Guerriero, Passive microwave remote sensing of forest: A model investigation, *IEEE Transaction on Geoscience and Remote Sensing*, 34, 433-443, 1996.

Frison, P.-L., E. Mougin, and P. Hiernaux, Observations and interpretation of seasonal ERS-1 wind scatterometer data over Northern Sahel (Mali), *Remote Sensing of the Environment*, 63, 233-242, 1998.

Frison, P.-L., and E. Mougin, Use of ERS-1 wind scatterometer data over land surfaces, *IEEE Transaction on Geoscience and Remote Sensing*, 34, 550-560, 1996 a.

Frison P.-L., and E. Mougin, Monitoring global vegetation dynamics with ERS-1 wind scatterometer data, *International Journal of Remote Sensing*, 17, 3201-3218, 1996 b.

Fung, I. Y., C. J. Tucker, and K.C. Prentice, Application of advanced very high resolution radiometer vegetation index to study atmosphere-biosphere exchange of CO2, *J. Geophys. Res.*, 92, 2999-3015, 1987.

Gausman, H. W., Leaf reflectance of near-infrared, *Photogram. Engr.*, 40, 183-191, 1974.

Giddings, L., and B. J. Choudhury, Observation of hydrological feature with Nimbus-7 37GHz data applied to South America, *International Journal of Remote Sensing*, 10, 1673-1686, 1989.

Gutman, G. G., On the use of long-term global data of land reflectances and vegetation indices from the advanced very high resolution radiometer, *J. Geophys. Res.*, 104, 6241-6255, 1999.

Hewison, T. J., Airborne measurements of land surface emissivity at millimeter wavelength, *IEEE Transaction on Geoscience and Remote Sensing*, submitted, 2000.

Holben, B. N., Characteristics of maximum-value composite images from temporal AVHRR data, *International Journal of Remote Sensing*, 7, 1417-1434, 1986.

Hollinger, J. P., R. Lo, G. Poe, R. Savage and J. Pierce, Special Sensor Microwave/Imager user's guide, Nav. Res. Lab. Washington, D. C., 1987.

Hollinger, J. P., J. L. Pierce and G. A. Poe, SSM/I instrument evaluation, *IEEE Transaction on Geoscience and Remote Sensing*, 28, 781-790, 1990.

Huffman, G. J., GPCP version 1 combined precipitation data set, SSAI, Lab. for Atmos., Natl. Aeronaut. and Space. Admin., Goddard Space Flight Cent., Greenbelt, Md., 1996.

James, M. E., and S. N. V. Kalluri, The Pathfinder AVHRR land data set: An improved coarse resolution data set for terrestrial monitoring, *International Journal of Remote Sensing*, 15, 3347-3364,1994.

Justice, C. O., J. R. Townshend and B. J. Choudhury, Comparison of AVHRR and SMMR data for monitoring vegetation phenology on a continental scale, *International Journal of Remote Sensing*, 10, 1607-1632, 1989.

Justice, C. O., T. F. Eck, D. Tanre, and B. N. Holben, The effect of water vapor on the normalized difference vegetation index derived for the Sahelian region from NOAA AVHRR data, *International Journal of Remote Sensing*, 12, 1165-1187, 1991.

Kalnay, E. et al., The NCEP/NCAR 40-year reanalysis project, *Bull. Am. Meteorol. Soc.*, 77, 437-470, 1996.

Karam, M. A., F. Amar, A. K. Fung, E. Mougin, A. Lopes, D. M. Le Vine, and A. Beaudoin, A microwave polarimetric scattering model for forest canopies based on vector radiative transfer theory, *Remote Sensing of the Environment*, 53, 16-30, 1995.

Kennett, R. G., and F. K. Li, Seasat over land scatterometer data. Part I: Global overview of the Ku-band backscatter coefficients, *IEEE Transaction on Geoscience and Remote Sensing*, 27, 592-605, 1989.

Kerr, Y. H., and E. G. Njoku, On the use of passive microwave at 37GHz in remote sensing of vegetation, *International Journal of Remote Sensing*, 14, 1931-1943, 1993.

Kerr, Y. H., and R. Magani, Use of the ERS-1 wind-scatterometer data over land surfaces: Arid and semi-arid lands, *Proc. 2nd ERS-1 Symposium*, Hamburg, Germany, Oct. 11-14, 383-388, 1993.

Knipling, E. B., Physical and physiological basis for the reflectance of visible and near-infrared

radiation from vegetation, *Remote Sensing of the Environment*, 1, 155-159, 1970.

Kohonen, T., Self-organization and associative memory, Springer-Verlag, 1984.

Marticorena, B., G. Bergametti, B. Aumont, Y. Callot, C. N'Doumi, and M. Legrand, Modeling the atmospheric dust cycle, 2, Simulation of Saharan dust sources, *J. Geophys. Res.*, 102, 4387-4404, 1997.

Matthews, E., Global vegetation and land use: new high-resolution data bases for climate studies, *Journal of Climate and Applied Meteorology*, 22, 474-486, 19' 3.

Matzler, C., Seasonal evolution of microwave radiation from an oat field, *Remote Sensing of the Environment*, 31, 161-173, 1990.

Moulin, S., L. Kergoat, N. Viovy, and G. Dedieu, Global-scale assessment of vegetation phenology using NOAA/AVHRR satellite, *Journal of Climate*, 10, 1154-1170, 1997.

Myneni, R. B., C. J. Tucker, G. Asrar, and C. D. Keeling, Interannual variations in satellite-sensed vegetation index data from 1981 to 1991, *J. Geophys. Res.*, 103, 6145-6160, 1998.

Owe, M., A. A. Van de Griend, R. de Jeu, J. J. de Vries, E. Seyhan, E. T. Engman, Estimating soil moisture from satellite microwave observations: Past and ongoing project, and relevance to GCIP, *J. Geophys. Res.*, 104, 19735-19742, 1999.

Pinty, B. and G. Szejwach, A new technique for inferring surface albedo from satellite observations, *Journal of Climate and Applied Meteorology*, 24, 741-750, 1985.

Prigent, C., W. B. Rossow, and E. Matthews, Microwave land surface emissivities estimated from SSM/I observations, *J. Geophys. Res.*, 102, 21867-21890, 1997.

Prigent, C., W. B. Rossow and E. Matthews, Global maps of microwave land surface emissivities: Potential for land surface characterization, *Radio Sci.*, 33, 745-751, 1998.

Prigent, C., W. B. Rossow, E. Matthews, and B. Marticorena, Microwave radiometric signatures of different surface types in deserts, *J. Geophys. Res.*, 104, 12147-12158, 1999.

Prigent, C.,J.-P. Wigneron, W. B. Rossow, and J. R. Pardo-Carrion, Frequency and angular variations of land surface microwave emissivities: Can we estimate SSM/T and AMSU emissivities from SSM/I emissivities, *IEEE Transaction on Geoscience and Remote*

Sensing, in press, 2000.

Rossow, W. B., and R. A. Schiffer, ISCCP cloud data products, *Bull. Am. Meteorol. Soc.*, 72, 2-20, 1991.

Rossow, W. B., A. W. Walker, D. E. Beuschel, and M. D. Roiter, International Satellite Cloud Climatology Project (ISCCP): Document on new cloud datasets, NASA Goddard Inst. for Space Stud., New York, 1996.

Sinclair, T. R., R. M. Hoffer, and M. M. Schreiber, Reflectance and internal structure of leaves from several crops during a growing season, *Agronomy Journal*, 63, 864-867, 1971.

Scott, D., P. H. Menalda, and R. W. Brougham, Spectral analysis of radiation transmitted and reflected by different vegetations, *New Zealand Journ. Botanic*, 6, 427-449, 1968.

Sellers, P. J., C. J. Tucker, G. J. Collatz, S. O. Los, C. O. Justice, D. A. Dazlich, and D. A. Randall, A global 1-deg by 1-deg NDVI data set for climate studies. Part 2. The generation of global fields of terrestrial biophysical parameters from the NDVI, *International Journal of Remote Sensing*, 15, 3519-3545, 1994.

Sellers, P. J., S. O. Los, C. J. Tucker, C. O. Justice, D. A. Dazlich, G. J. Collatz, and D. A. Randall, A revised land surface parameterization (SiB2) for atmospheric GCMs. Part II: The generation of global fields of terrestrial biophysical parameters from satellite data, *Journal of Climate*, 9, 706-737, 1996.

Sippel, S. J., S. K. Hamilton, J. M. Melack, and E. M. M. Novo, Passive microwave observations of inundation area and area/stage relation in the Amazon River floodplain, *International Journal of Remote Sensing*, 19, 3055-3074, 1998.

Tucker, C. J., Red and photographic infrared linear combinations for monitoring vegetation, *Remote Sensing of the Environment*, 8, 127-150, 1979.

Tucker, C. J., J. R. G. Townshend, and T. E, Goff, African land-cover classification using satellite data, *Science*, 227, 369-375, 1985.

Tucker, C. J., Comparing SMMR and AVHRR data for drought monitoring, *International Journal of Remote Sensing*, 10, 1663-1672, 1989.

Ulaby, F. T., R. K. Moore and A. K. Fung, *Microwave Remote Sensing, Active and Passive*, vol. 3, Artech House, Reading, Ma., 1986.

Vinnikov, K. Y., A. Robock, S. Qiu, J. K. Entin, M. Owe, B. J. Choudhury, S. E. Hollinger, and E. G. Njoku, Satellite remote sensing of soil moisture in Illinois, United States, *J. Geophys. Res.*, 104, 4145-4168, 1999.

Wagner, W., G. Lemoine, and M. Borgeaud, A study of vegetation cover effects on ERS scatterometer data, *IEEE Transaction on Geoscience and Remote Sensing*, 37, 938-947, 1999a.

Wagner, W., J. Noll, M. Borgeaud, and H. Rott, Monitoring soil moisture over the Canadian prairies with the ERS scatterometer, *IEEE Transaction on Geoscience and Remote Sensing*, 37, 206-216, 1999b.

Wigneron, J.-P., J.-C. Calvet, Y. Kerr, A. Chanzy, and A. Lopes, Microwave emission of vegetation: sensitivity to leaf characteristics, *IEEE Transaction on Geoscience and Remote Sensing*, 31, 716-726, 1993.

Wigneron, J.-P., D. Guyon, J.-C. Calvet, G. Courrier, and N. Bruguier, Monitoring coniferous forest characteristics using a multifrequency (5-90 GHz) microwave radiometer, *Remote Sensing of the Environment*, 60, 299-310, 1997.

Wismann, K. Boehnke, and C. Schullius, Radar signatures of land surfaces measured by the ERS-1 scatterometer, *Proc. 2nd ERS-1 Symposium*, Hamburg, Germany, Oct. 11-14, 405-410, 1993.

C. Prigent, F. Aires, and W. B. Rossow, NASA Goddard Institute for Space Studies, 2880 Broadway, New York, N.Y. 10025, USA, e-mail: cprigent@giss.nasa.gov

E. Matthews, NASA Goddard Institute for Space Studies, 2880 Broadway, New York, N.Y. 10025

Received _____

Figure 1. August 1992 monthly-mean satellite products presented on an equal area grid of $0.25° \times 0.25°$ at the equator: a) NDVI (AVHRR) from the Pathfinder, b) emissivity polarization differences (vertical-horizontal) at 37 GHz from SSM/I, c) ERS-1 scatterometer backscattering coefficient in dB; d) Simplified version of the *Matthews* [1993] vegetation classification (10 classes) at a spatial resolution of $1° \times 1°$.

Figure 2. Histograms of the different observations for 4 major vegetation types, for the northern hemisphere. For a given observation, histograms are normalized to have the same area. Evergreen and deciduous forests have been grouped, as well as evergreen and deciduous woodlands. Are only considered pixels with less than 20% cultivation intensity. The number of pixels is indicated.

Figure 3. For the northern hemisphere and for the different observations, histograms of 6 vegetation types, for three months that correspond to different vegetation stages. Areas where the cultivation intensity is larger than 20% are excluded as well as pixels that are snow covered for at least one month. The number of pixels is indicated. Numbers indicate the mean difference between August 1992 and February 1993, along with the standard deviations in parenthesis.

Figure 4. Scatterplots of NDVI, VIS and NIR reflectances, and radar backscattering versus the high cloud amount derived from ISCCP, for $6° \times 6°$ in the African rain forest (3S 3N; 17E 23E) for a year. The correlation coefficient is indicated.

Figure 5. For three grassland types with different woody cover, time series over a year (July 1992- June 1993) of the mean response of three selected observations (AVHRR NDVI, ERS-1 scatterometer backscattering coefficient in dB, SSM/I emissivity polarization difference at 37 GHz). The standard deviation is also plotted. Pixels that are snow covered for at least one month during the year are excluded. Results are presented for the northern and southern hemispheres and the number of pixels is indicated.

Figure 6. Comparisons of AVHRR NDVI, ERS-1 backscattering coefficient, and SSM/I emissivity polarization difference at 37 GHz along a cross section at 20E from 20N to the equator, for August 1992 and February 1993. The vegetation class in *Matthews'* classification is indicated for each degree. For 5 specific sites along the cross section, the full seasonal cycle is given with the precipitation rate in mm/day extracted from the GPCP data set. For comparison purposes, all the values are normalized between 0 and 1 that corresponds to variations from 0 to 1 for the NDVI, from -26 dB to -6 dB for the ERS-1 backscattering coefficient, from 0.15 to 0.0 for the SSM/I emissivity polarization difference, and from 0mm/day to 12mm/day for the rain rate.

Figure 7. Scatterplots of all possible pairs of observations for the AVHRR NDVI, the ERS-1 backscattering coefficient and the SSM/I emissivity polarization difference at 37 GHz for four major vegetation types. Results are presented for the southern hemisphere, during summer (February 1993). For each scatter plot, the population contours at 0.5% and 0.2% are drawn.

Figure 8. For August 1992, cluster map derived from the *Kohonen* scheme.

Figure 9. For each observation, value of the prototype in each cluster (solid line), along with the standard deviation around this prototype in the cluster (dashed line). For passive microwaves, standard deviations are indicated for 19 GHz only. The standard deviations for the other channels are similar.

Figure 10. Response of each instrument over wetlands in the Amazon rain forest, for every other month between July 1992 and June 1993. The precipitation is also indicated as given by GPCP.

Table 1. Vegetation Types

Vegetation types				
31 classes	10 classes	Pixels N hem.	Pixels S hem.	Description
1	1	5942	10149	tropical evergreen rain forest, mangrove
2	3	3654	621	tropical/subtropical evergreen seasonal broadleaved forest
3	1	0	231	subtropical evergreen rainforest
4	3	0	479	temperate/subpolar evergreen rainforest
5	3	780	134	temperate evergreen seasonal broadleaved forest, summer rain
6	5	322	236	evergreen broadleaved sclerophyllous forest, winter rain
7	3	618	0	tropical/subtropical evergreen needleleaved forest
8	3	11921	0	temperate/subpolar evergreen needleleaved forest
9	2	1823	1647	tropical/subtropical drought-deciduous forest
10	2	5559	95	cold-deciduous forest, with evergreens
11	2	4598	0	cold-deciduous forest, without evergreens
12	8	718	2624	xeromorphic forest/woodland
13	5	695	1408	evergreen broadleaved sclerophyllous woodland
14	5	3227	0	evergreen needleleaved woodland
15	4	1767	3438	tropical/subtropical drought-deciduous woodland
16	4	3240	0	cold-deciduous woodland
17	8	1357	272	evergreen broadleaved shrubland/thicket and dwarf shrubland
18	8	817	41	evergreen needleleaved or microphyllous shrubland/thicket
19	8	844	214	drought-deciduous shrubland/thicket and dwarf shrubland/thicket
20	8	601	0	cold-deciduous subalpine/subpolar shrubland and dwarf shrubland
21	8	6258	5279	xeromorphic shrubland/dwarf shrubland
22	7	9482	8	arctic/alpine tundra/mossy bog
23	6	3781	4587	tall/medium/short grassland with 10-40% tree cover
24	6	3168	1808	tall/medium/short grassland with <10% tree or tuft-plant cover
25	6	8839	3374	tall/medium/short grassland with shrub cover
26	6	598	438	tall grassland, no woody cover
27	6	560	436	medium grassland, no woody cover
28	6	4872	2724	meadow/short grassland, no woody cover
29	6	359	0	forb formation
30	9	18187	1934	desert (bare soil)
31	10	24965	2896	cultivation

The 31 vegetation classes are defined by *Matthews* [1983]. The number of equal area pixels of $0.25° \times 0.25°$ at the equator is indicated for each vegetation type and for each hemisphere. Each pixel surface is 773 km^2. The 10-class vegetation classification is also defined, in relation to the *Matthews'* original classification.

Fig. 1

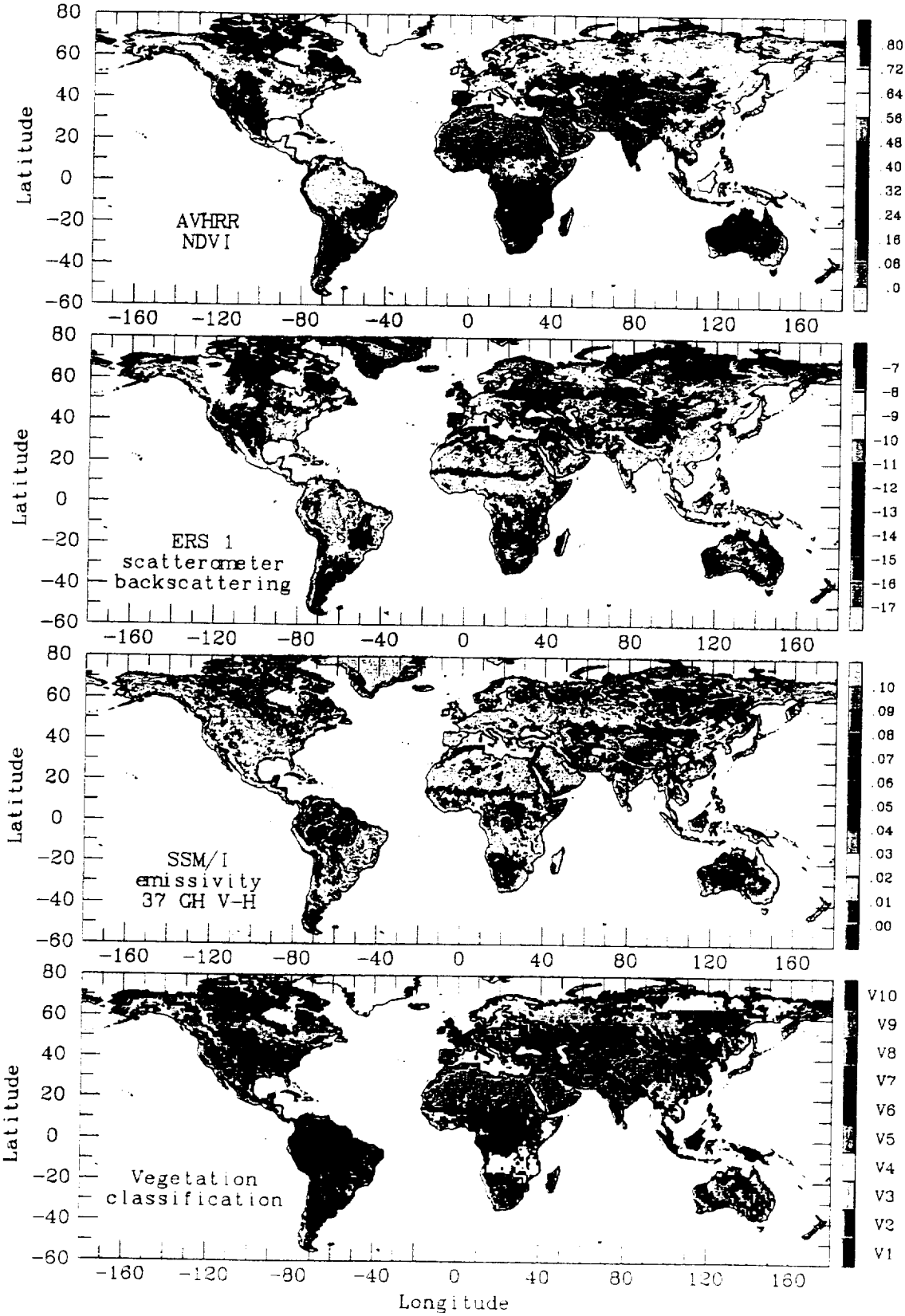

August 92

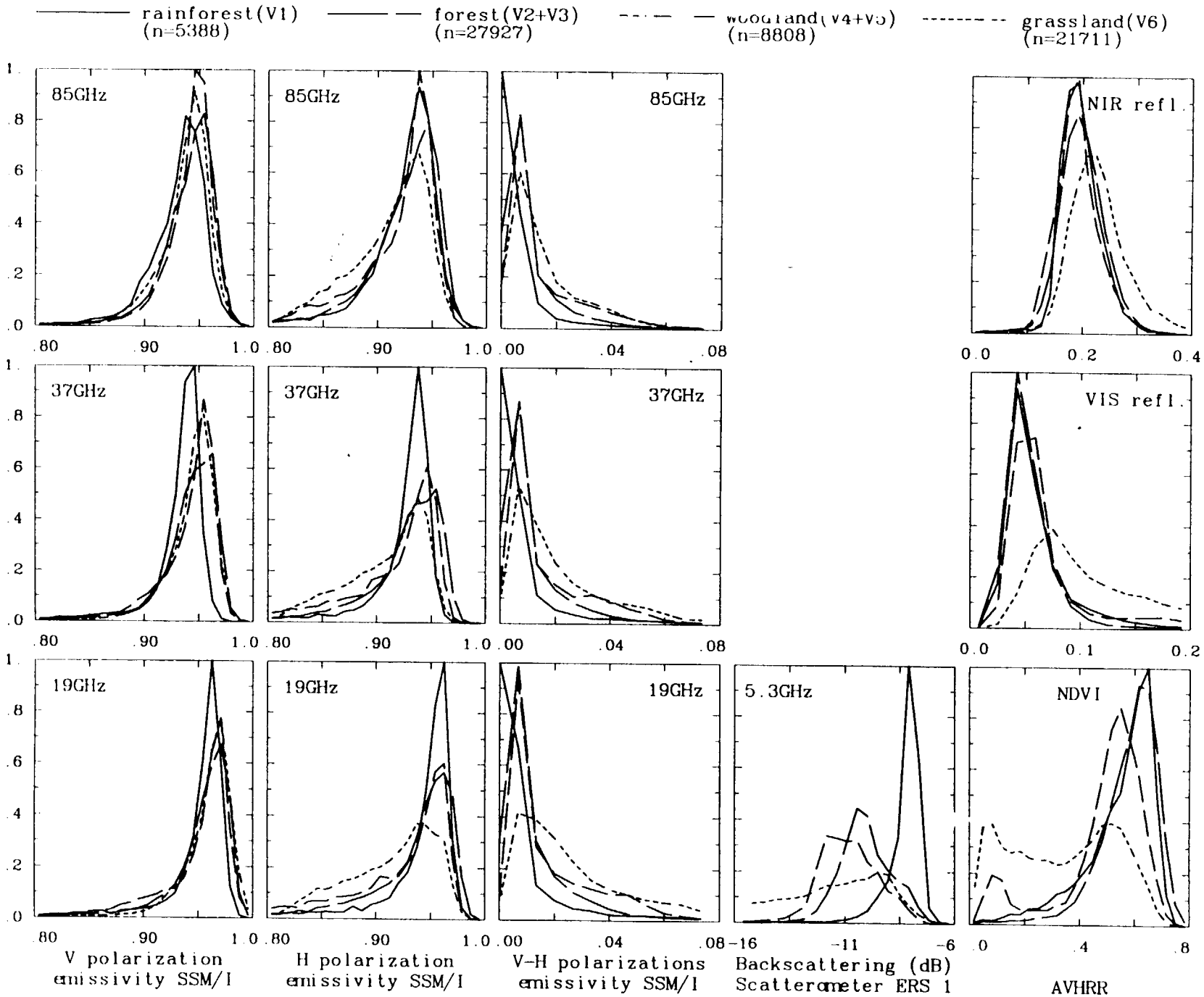

Northern Hemisphere - August 1992

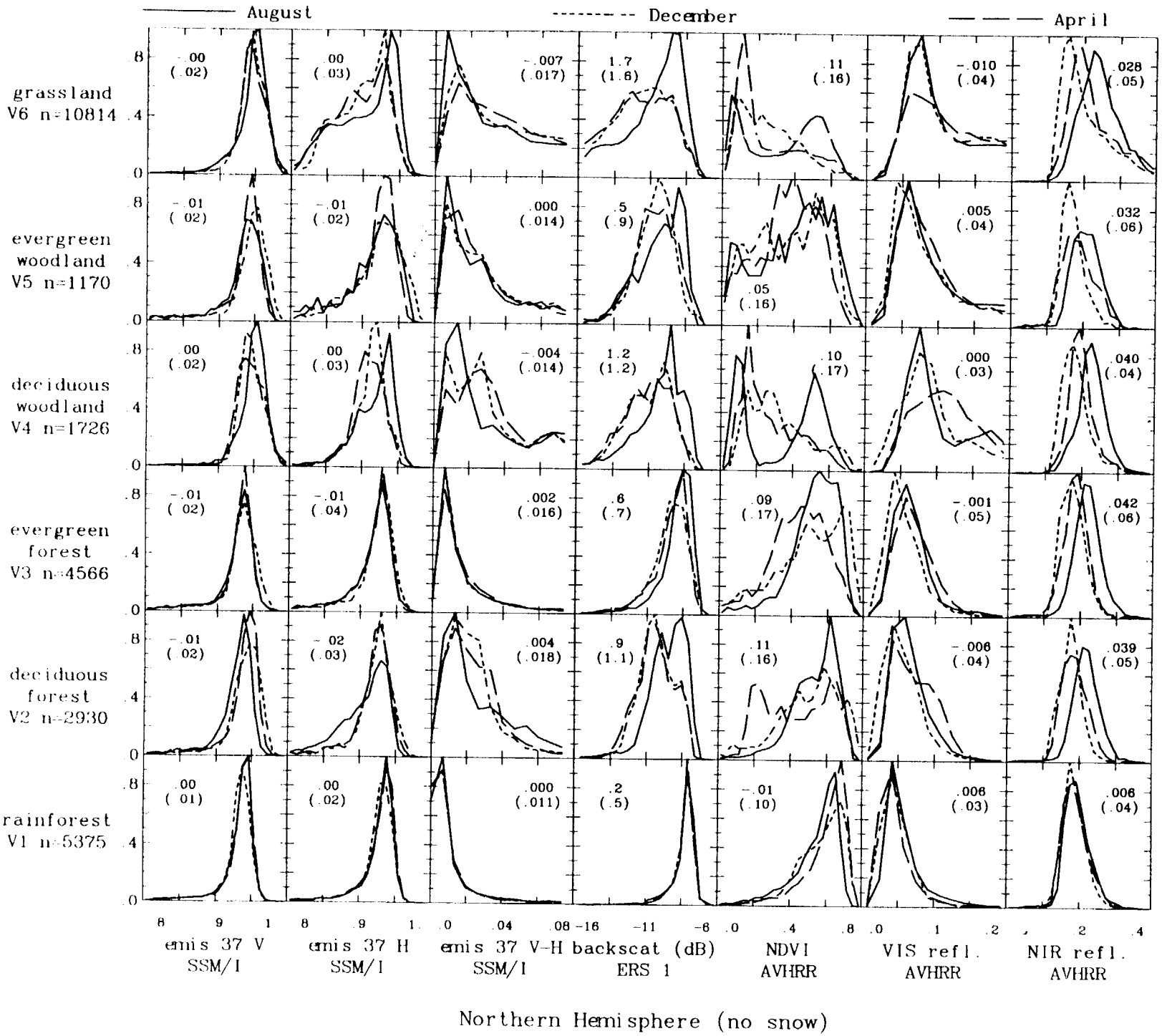

Northern Hemisphere (no snow)

Fig 4

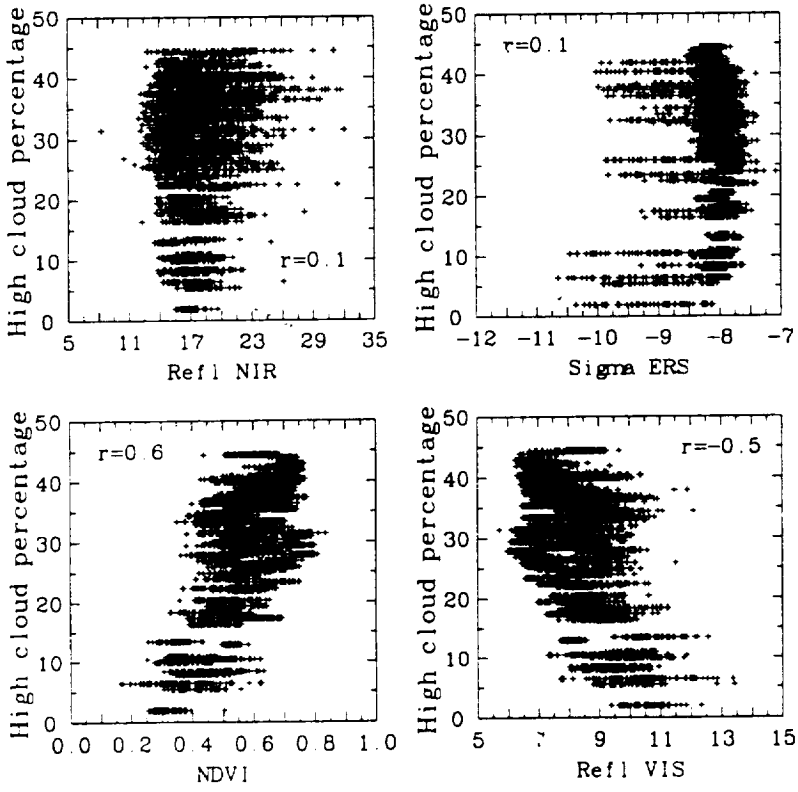
High cloud percentage
0
10
20
30
40
50
5
11
17
23
29
35
Refl NIR
r=0.1
High cloud percentage
0
10
20
30
40
50
-12
-11
-10
-9
-8
-7
Sigma ERS
r=0.1
High cloud percentage
0
10
20
30
40
50
0.0
0.2
0.4
0.6
0.8
1.0
NDVI
r=0.6
High cloud percentage
0
10
20
30
40
50
5
9
11
13
15
Refl VIS
r=-0.5

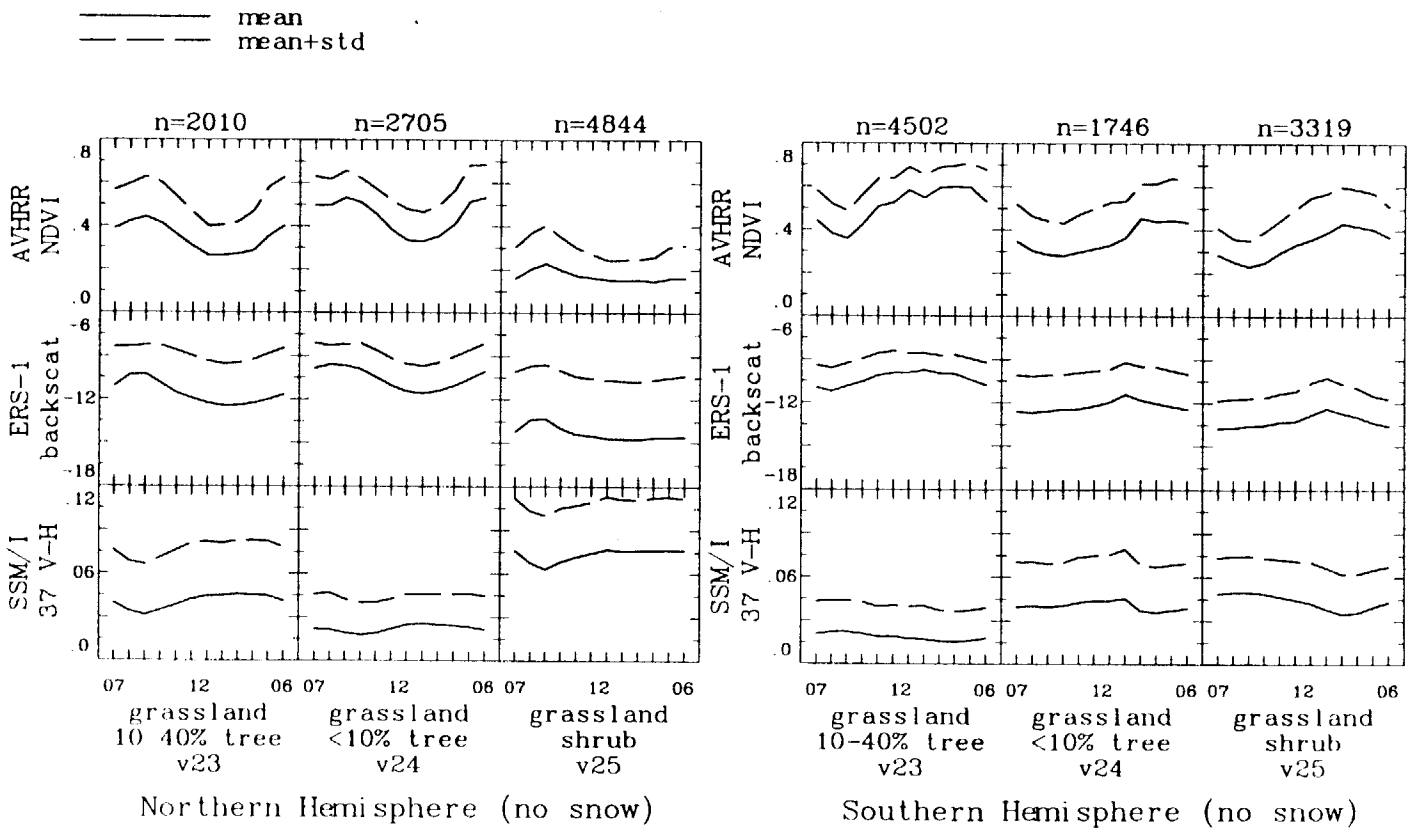
mean
mean+std
n=2010
n=2705
n=4844
n=4502
n=1746
n=3319
AVHRR NDVI
ERS-1 backscat
SSM/I 37 V-H
.8
.4
.0
-6
-12
-18
.12
.06
.0
07
12
06
grassland 10 40% tree v23
grassland <10% tree v24
grassland shrub v25
grassland 10-40% tree v23
Northern Hemisphere (no snow)
Southern Hemisphere (no snow)

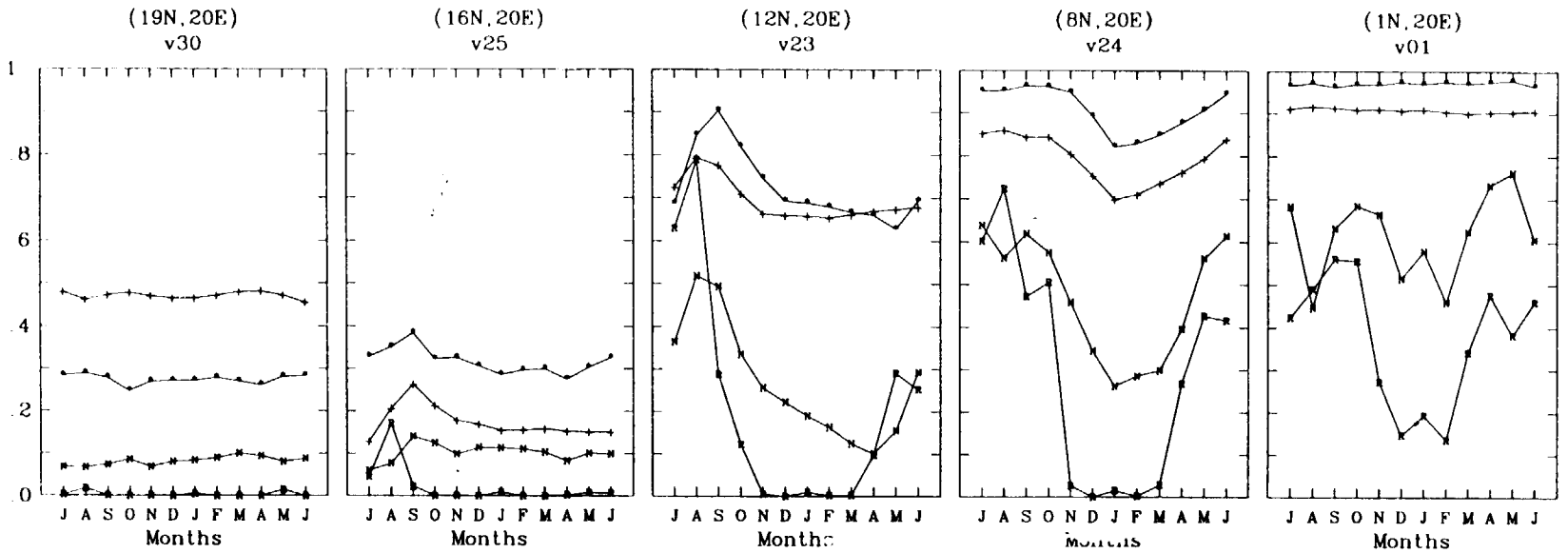

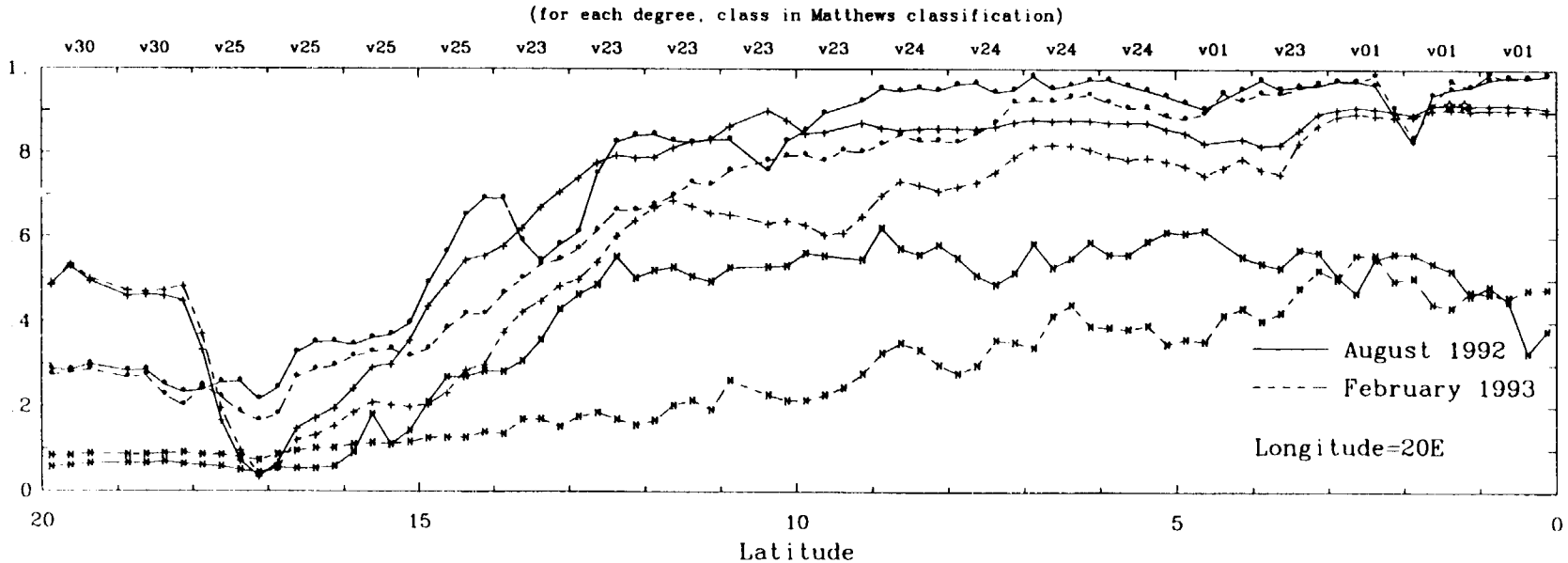

N AVHRR NDVI; + ERS-1 backscattering coef; * SSM/I emissivity V-H 37 GHz; R rain in mm/day (GPCP)

Fig 7

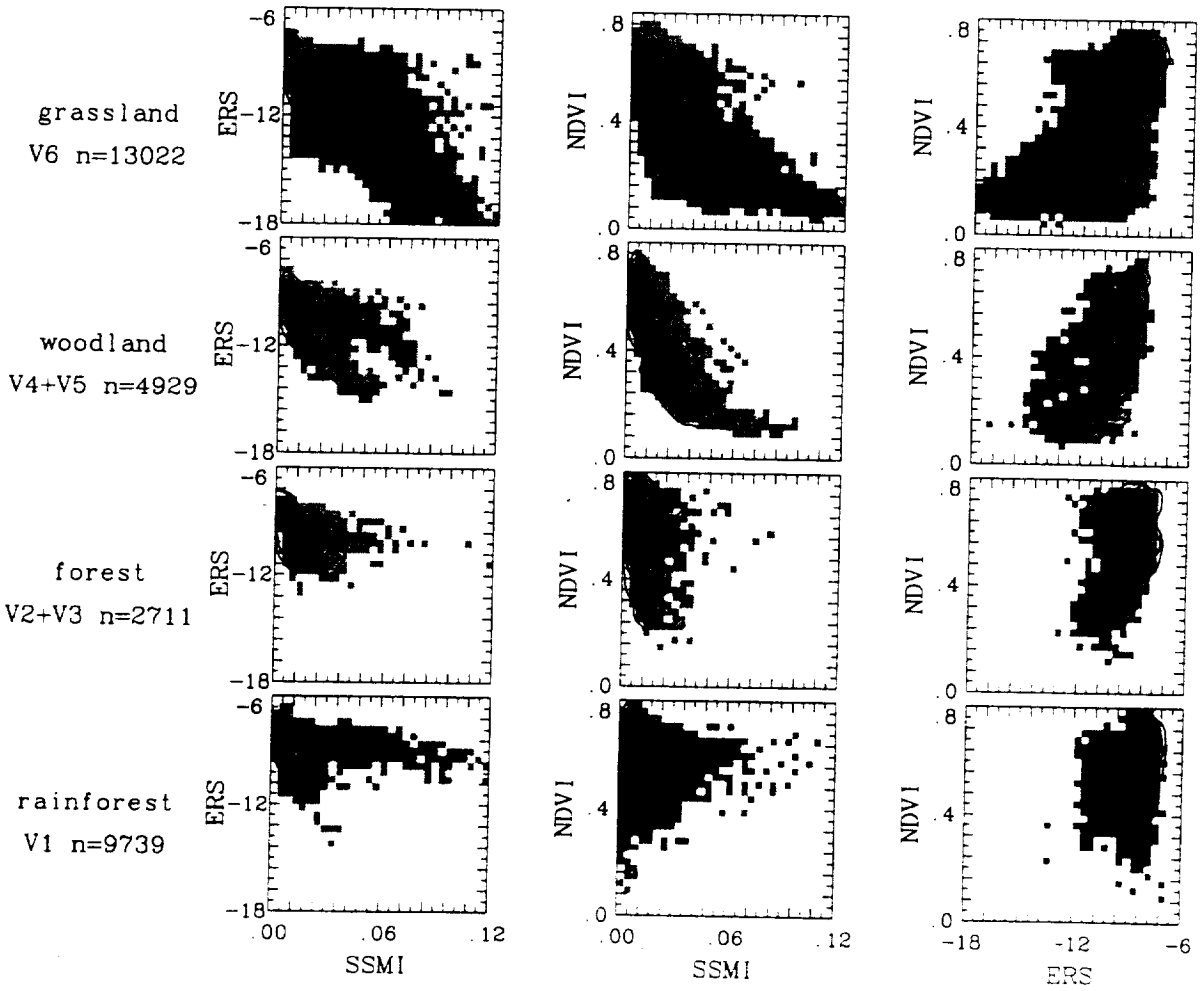

South Hemisphere - February

Fig 8

Cluster SSMI ERS1 AVHRR
August 1992

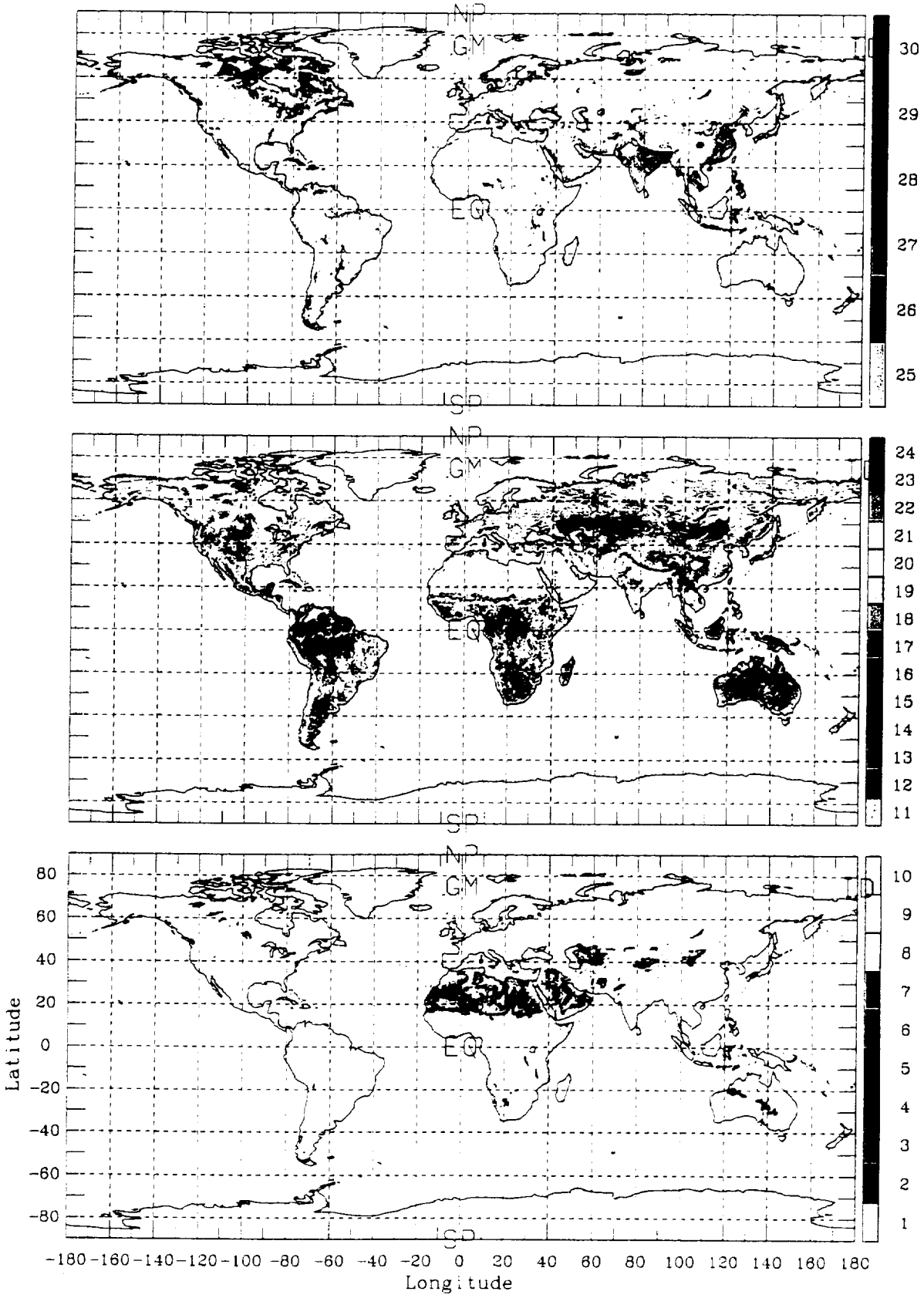

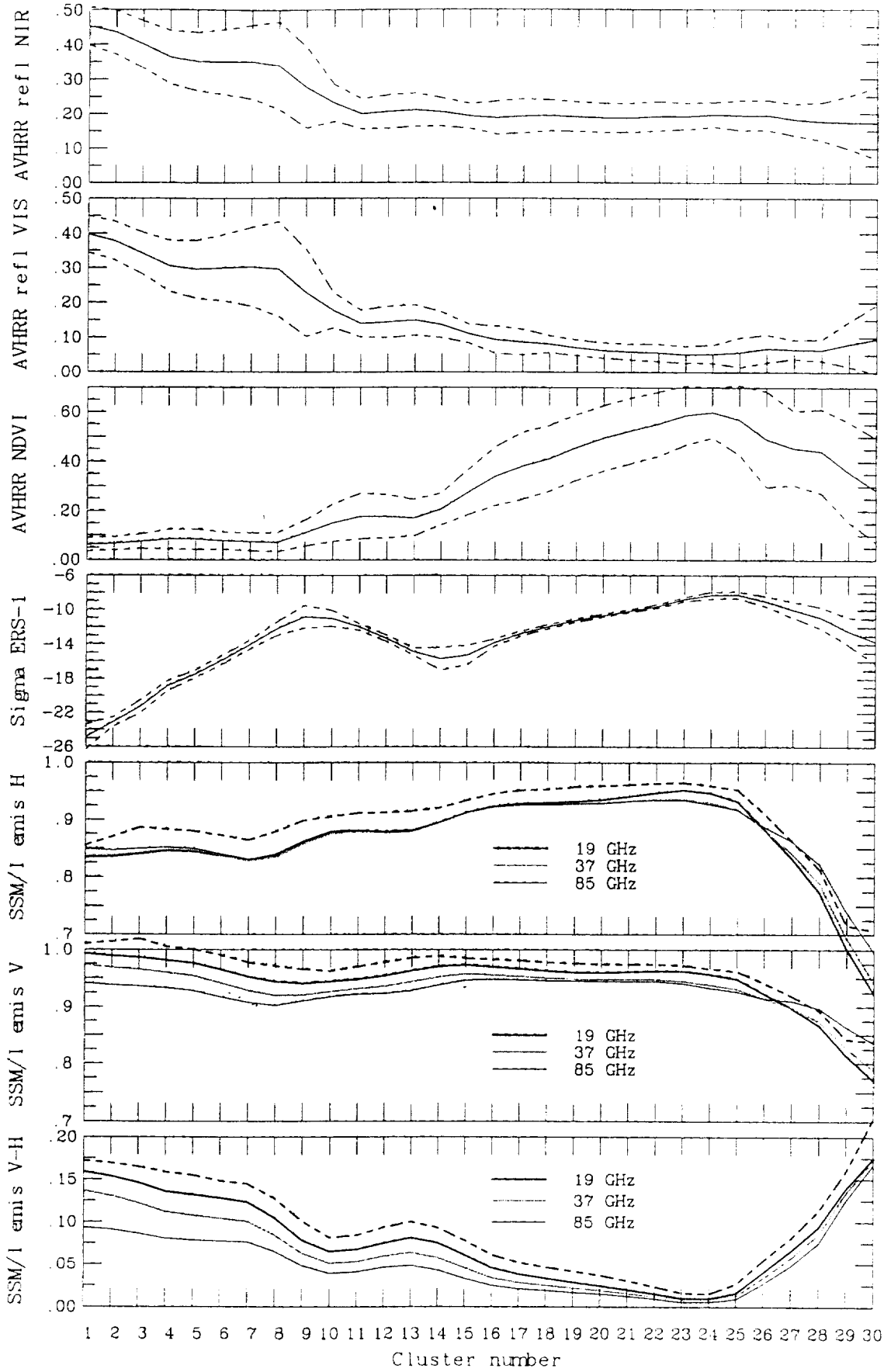
AVHRR refl NIR
.50
.40
.30
.20
.10
.00
AVHRR refl VIS
.50
.40
.30
.20
.10
.00
AVHRR NDVI
.60
.40
.20
.00
Sigma ERS-1
-6
-10
-14
-18
-22
-26
SSM/I emis H
1.0
.9
.8
.7
19 GHz
37 GHz
85 GHz
SSM/I emis V
1.0
.9
.8
.7
19 GHz
37 GHz
85 GHz
SSM/I emis V-H
.20
.15
.10
.05
.00
19 GHz
37 GHz
85 GHz
1 2 3 4 5 6 7 8 9 10 11 12 13 14 15 16 17 18 19 20 21 22 23 24 25 26 27 28 29 30
Cluster number

07/92
09/92
11/92
01/93
03/93
05/93
lat
-4 -3 -2 -1 0
lon
-68 -67 -66 -65 -64
e37V
e37H
e37V-H
SigERS
NDVI
Precip
0 4 8 12
mm/day
07/92
09/92
11/92
01/93
03/93
05/93
0.00 0.01 0.02 0.03 0.04 0.05 0.06 0.07 0.08 0.09 0.10
0.80 0.82 0.84 0.86 0.88 0.90 0.92 0.94 0.96 0.98 1.00
eV or eH
eV-H
-.2 -.1 0.0 0.1 0.2 0.3 0.4 0.5 0.6 0.7 0.8
-12.0 -11.5 -11.0 -10.5 -10.0 -9.5 -9.0 -8.5 -8.0 -7.5 -7.0
NDVI
SigERS

Amazon